Biosensors and Bioelectronics 124–125 (2019) 122–128

Contents lists available at ScienceDirect

Biosensors and Bioelectronics

journal homepage: www.elsevier.com/locate/bios

Single step grown MoS_2 on pencil graphite as an electrochemical sensor for guanine and adenine: A novel and low cost electrode for DNA studies

Nandimalla Vishnu, Sushmee Badhulika*

Department of Electrical Engineering, Indian Institute of Technology Hyderabad, Kandi 502285, Telangana, India

ARTICLE INFO

Keywords:
Adenine
Guanine
Pencil
Molybdenum disulfide
Calf-thymus DNA

ABSTRACT

Herein we report a simple, one-step approach to prepare a low-cost and binder free MoS_2-pencil graphite electrode (i.e., MoS_2-PGE) for the electrochemical oxidation of DNA nucleobases i.e., guanine (G) and adenine (A) in physiological pH (7.4) buffer solution. MoS_2-PGE was synthesised by hydrothermal method and the morphology of such hybrid was characterized by field emission scanning electron microscopy, X-ray diffraction, Raman and X-ray photoelectron spectroscopy. In cyclic voltammetry, MoS_2-PGE displays two well-seprated and well-defined irreversible peaks at 0.58 and 0.90 V for electrochemical oxidation of G and A respectively when compared to bare PGE. Likewise, differential pulse voltammetry of MoS_2-PGE showed well-seprated and sharp peak current responses for G and A at 0.56 V and 0.85 V respectively. Under optimized conditions, DPV was further adopted for simultaneous and separation-free determination of G and A in physiological pH. MoS_2-PGE shows good stability with linear range of 15–120 μM and 15–120 μM for G and A detection respectively. Obtained sensitivity and limit of detection (signal-to-noise = 3) are comparable with the previous literature. As an immediate practical applicability, MoS_2-PGE was used for quantification of G and A concentration in calf-thymus DNA and detected ratio of G and A (i.e., [G]/[A]) ratio is 0.85. The current approach provides a new avenue towards the development of affordable electrodes for a wide range of bioanalytical applications.

1. Introduction

The human chromosome is a biopolymer that contains a complex combination of deoxyribonucleic acid (DNA). DNA assist the development of biological function by replication and transcription of genetic information through unique combinations of guanine (G), adenine (A), thymine (T), and cytosine (C) nucleobases (Hirao et al., 2012; Ng and Khor, 2017; Wetmur, 1991). Thus the naive combination of these DNA bases are crucial in preservation of genetic information and organism function (Ng and Khor, 2017). Unfortunately, lifestyle stress, UV exposure, and consumption of carcinogenic chemicals and food preservatives roots damage to DNA by translocations or deletions or insertions of the nucleobases (Yang et al., 2015a). Delay in diagnosis may cause mutations and weakens the health of organism by deregulation of gene expression, tumorigenesis and cell death/apoptosis (Pradhan et al., 2018). Thus, to find an appropriate way to determine the concentration of G, A, T and C is very significant for bioanalytical chemistry and life-sciences.

Various analytical methods like HPLC, MS, electrophoresis and electrochemical methods have been developed for the determination of these four DNA bases (Li et al., 2016; Ng and Khor, 2017). Among these methods, electrochemical methods are much advantageous in terms of simplicity, time and cost involved. For instance, chromatography based techniques are selective, precise and exact; but the chromatographic approach need the complex sample preparation steps like enrichment of DNA or its derivatization which are cumbersome and laborious. In addition, methods based electrochemistry offer simple, fast and sensitive approach for selective and simultaneous detection of DNA base pairs (Chu et al., 2016; Fan et al., 2010; Li et al., 2016; Ng and Khor, 2017; Pradhan et al., 2018; Randviir and Banks, 2012; Yang et al., 2015a, 2015b; Yin et al., 2010). Till date, several modified electrodes have proved to be efficient in improving the response of analytes and many materials, including organic polymer film (Yang et al., 2015a, 2015b), nanoparticles (Pradhan et al., 2018), carbon materials (Chu et al., 2016; Fan et al., 2010; Li et al., 2016; Randviir and Banks, 2012; Yin et al., 2010) and so on, have been used for determination of purine (G and A) bases. Note that, electrochemical detection of pyrimidine bases (C and T) at higher oxidation potentials result in large back ground currents in blank solutions (Randviir and Banks, 2012). Thus, most of the reported electrodes are limited their analyses with electrochemical detection of purines (G and A) only. However, G pair selectively with C and A with T as per the Watson-Crick DNA model and

* Corresponding author.
E-mail address: sbadh@ith.ac.in (S. Badhulika).

https://doi.org/10.1016/j.bios.2018.08.055
Received 28 June 2018; Received in revised form 23 August 2018; Accepted 23 August 2018
Available online 24 August 2018
0956-5663/

the amount of the nucleobases are equivalent to one another as [G] = [C] and [A] = [T] (Li et al., 2016). Moreover, the ratio between purine (i.e., [G]/[A]) or pyrimidine (i.e., [C]/[T]) bases should range in 0.8–1.0 in a healthy DNA double helical structure (Ng and Khor, 2017). Abnormalities in the ratio of DNA base pair could be an indicator for cancer, ageing and other diseases (Hirao et al., 2012). For instance, the value of [G]/[A] for breast cancer patient's blood DNA was found to be 0.6 (Arvand et al., 2018) which is in contrast to the standard value of healthy DNA. Thus, low-cost material and sensitive method is crucial for simultaneous and separation-free analyses of G and A and such analyses are vital to determine the ratio of DNA's nucleobases.

In this regard, two dimensional (2D) nanomaterials with distinctive structure and physicochemical properties have attained wide consideration in electrochemical based sensors, energy conversion and storage devices (Barua et al., 2018; Huang et al., 2015; Zhang et al., 2015). Owing to higher electron mobility, ionic conductivity, active sites and layer dependent band gap, molybdenum disulfide (MoS_2), a transition metal dichalcogenides (TMDs), has been found to be an attractive 2D nanomaterial for development of electrochemical sensors (Nandi et al., 2017; Zhang et al., 2015). Furthermore, MoS_2 is an inorganic analogue of graphene comprises of S-Mo-S triple layers which are held together by weak vanderwaals interactions (Sun et al., 2016). Herein, we report for the first time the development of an ultra-low cost electrode for the electrochemical sensing of DNA base pairs (G and A) using a pencil graphite electrode and MoS_2, whereas MoS_2 was hydrothermally grown on commercially available pencil graphite electrode. The as developed sensor displayed excellent analytical performance in terms of better sensitivity and lower limit of detection towards G and A. Finally, the practicability of the proposed sensor was successfully demonstrated by electrochemical sensing of G and A in a real sample i.e., DNA from calf-thymus. Note that, electrochemical applications related to MoS_2 grown pencil graphite are unexplored yet. To the best of our knowledge, there are no such reports on a single step grown MoS_2-pencil graphite as an electrochemical sensor for G and A.

2. Experimental

2.1. Materials

Guanine, adenine, calf thymus double stranded DNA, sodium molybdate dihydrate ($Na_2MoO_4{\cdot}2H_2O$), thiourea (H_2NCSNH_2), disodium phosphate (Na_2HPO_4), monosodium phosphate (NaH_2PO_4) were procured from Sigma Aldrich and were used as received. Likewise, all the other analytical grade chemicals were used as received without any purification. Commercially available pencil (Camlin, India) procured from a local book store exists in campus. Aqueous solutions were prepared using DI water (18.2 MΩ) collected from a Millipore system (Merck). Unless otherwise mentioned, 0.1 M phosphate buffer solution (PBS) of pH 7.4 was used as a supporting electrolyte.

2.2. Electrochemical and material characterization

All electrochemical measurements like impedance spectroscopy (EIS), cyclic voltammetry (CV) and differential pulse voltammetry (DPV) were carried out using a CHI 660E electrochemical workstation, USA with 10 mL working volume. A 3 electrode system containing Silver/Silver Chloride with 3 M KCl acts as a reference electrode, Pt wire as counter electrode and pencil graphite electrode (PGE) or MoS_2 grown PGE (i.e., MoS_2-PGE) as working electrode were used. X-ray diffraction was carried out using D8 Advanced diffractometer from Bruker, Germany containing a Cu Kα source (λ = 1.5418 Å). Raman spectra were obtained using 532 nm laser probe on Agiltron Peakseeker Pro Raman Spectrometer. X-ray Photoelectron Spectroscopy (XPS) data was collected using ULVAC-PHI, model no. PHI5000VersaProbeII. Likewise, Field emission scanning electron microscope (FESEM) analyses was carried out with Zeiss EVO 18 (Germany). The optimal parameters for DPV based experiments are: Initial potential = 0.2 V; final potential = 1.1 V; increment potential = 0.004 V; amplitude = 0.05 V; pulse period = 0.5 s; pulse width = 0.2 s. All the analyses were performed in 25 ± 2 °C temperature.

2.3. Growth of MoS_2 on pencil rod

Simple and a facile hydrothermal method is used for direct growth of MoS_2 on PGE. For 0.5 h, a pencil rod (i.e., PGE) was immersed in a seed solution (0.2 g of thiourea (H_2NCSNH_2) and 0.1 g of sodium molybdate dihydrate ($Na_2MoO_4{\cdot}2H_2O$) in 10 mL DI water). After this, PGE was dried in a hot air oven at 80°C for 1 h. Afterwards, the seed layer covered PGE was transferred to a Teflon-lined stainless steel autoclave (50 mL) which contain 30 mL of nutrient solution (0.6 g of H_2NCSNH_2 and 0.3 g of $Na_2MoO_4{\cdot}2H_2O$ in 30 mL of DI water) and heated in a hot air oven at 200°C for 24 h. After cooling down to room temperature, the MoS_2 grown PGE (i.e., MoS_2-PGE) was dried at 70°C and extended for characterization studies. Note: Prior to the hydrothermal synthesis, the surface of PGE was mechanically smoothened by polishing with a silicon carbide water proof abrasive paper (1500 Cw).

2.4. Fabrication of electrochemical sensor

PGE was fabricated as per our previous reports (Vishnu et al., 2017, 2018). In brief, wooden part of commercially available pencil was carefully removed to obtain a graphite rod (3 × 70 mm). To maintain uniformity, outer surface of pencil graphite rod is wrapped with a non-conductive parafilm (Sigma Aldrich) by leaving the disc portion of bottom end (0.0707 cm^2). Note that, the electrochemical measurements by PGE was carried out after mechanical smoothening with silicon carbide based water proof abrasive paper (1500 Cw). Likewise, MoS_2-PGE was fabricated from MoS_2 grown pencil rod by covering with parafilm leaving the disc portion (bottom end) for the electrochemical analyses and top portion is for the electrical contact (Fig. 1).

2.5. Analyses of DNA base pairs

Contents of A and G were analysed after the denaturation process of double stranded DNA (Thangaraj et al., 2014). Briefly, 5 mg of DNA was added with 3 mL of 1 M hydrochloric acid for 1 h and placed in hot water bath (70 °C). After the digestion, the sample was neutralised with 1 M sodium hydroxide and made a final volume of 10 mL with pH 7.4 PBS. Obtained 10 mL was used for the quantification of base pairs by standard addition method.

3. Results and discussion

3.1. Physicochemical characterization

Hydrothermal growth of MoS_2 on PGE was achieved by a simple and facile process. During seeding layer formation thermodynamic barrier was reduced between PGE and the nutrient solution, so offering an analogous environment on the substrate for the MoS_2 growth. The nanoparticles formed on the PGE from the precursors of MoS_2 (sodium molybdate dihydrate, thiourea) and aggregate followed by the seeding layer formation. Under hydrothermal conditions, MoS_2 nanostructures develop from this seeding layer. The developed synthesis procedure is dissimilar from the recent MoS_2 report from our group where MoS_2 shows higher semiconducting 2H phase than the metallic 1T phase (Sahatiya et al., 2018). Due to the higher molar ratio of S and Mo precursors used for the growth of MoS_2 nanostructures, higher content of 1T phase than 2H phase was obtained in the MoS_2 grown in the current work. Since higher content of 1T phase in MoS_2 facilitates excellent conductivity, rapid electron-transfer kinetics with enhanced catalytic sites, MoS_2 grown PGE is enticing material for electrochemical sensing applications

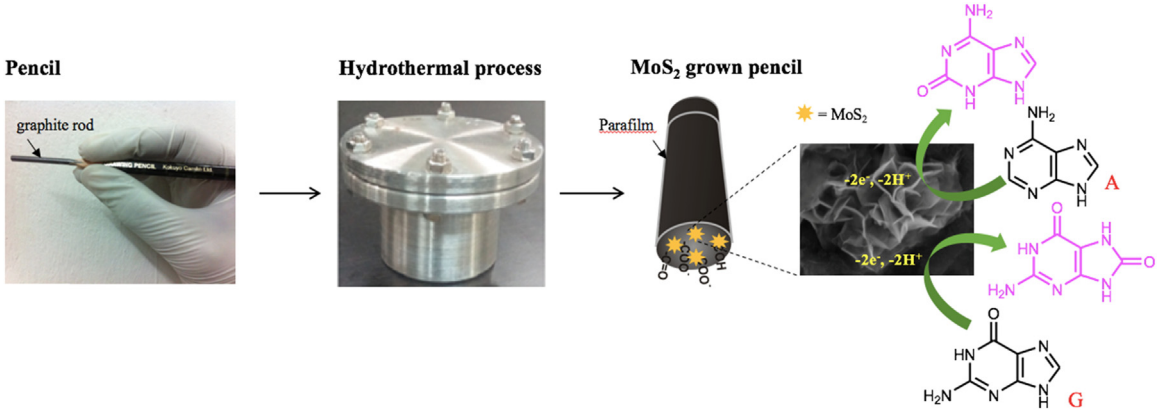

Fig. 1. Schematic illustration of the fabrication of MoS_2-PGE based electrochemical sensor for G and A; (1) formation of seeding layer, (2) hydrothermal growth of MoS_2 on PGE and (3) parafilm wrapped MoS_2-PGE electrode towards electrochemical oxidation of G and A.

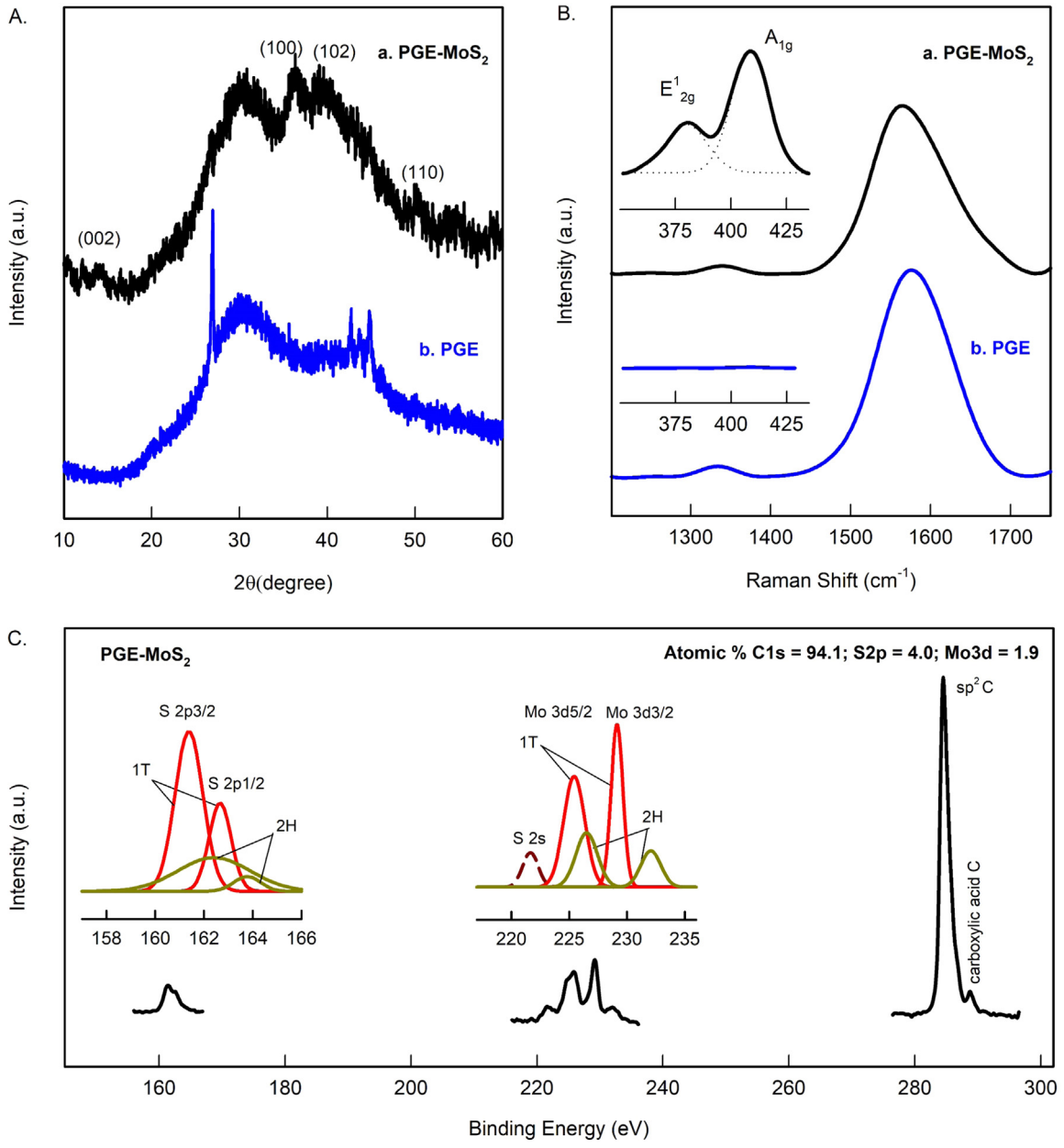

Fig. 2. (A) XRD (B) Raman and (C) XPS spectra of the MoS_2 grown PGE and its control sample.

Surface morphology of hydrothermally grown MoS_2-PGE was studied using FESEM. Fig. S1A is FESEM image of MoS_2-PGE marking on A4 paper at lower magnification where a flower-like morphology was noticed with an average size of ~ 0.4–2 μm. At higher magnification of FESEM of MoS_2 (Fig. S1B) shows that each MoS_2 flower contains a good number of interlaced nanosheets. Such nanosheets increase the MoS_2 surface area, thus, providing shorter diffusion lengths for electrolytic ions and high number of active sites which facilitates electrochemical detection of an analyte. Similarly, characterization by XRD and Raman spectroscopy of MoS_2-PGE and PGE were performed. Curve a of Fig. 2A displays the XRD spectra of MoS_2-PGE. Availability of a diffraction peak (002) at 13.4° indicates the presence of few layered MoS_2 (Sahatiya et al., 2018) on surface of PGE. Peaks at 31.6°, 35.6° and 54.3° are attributed to MoS_2 crystallographic planes (Li et al., 2015; Sun et al., 2016). In precise, diffractions peaks at 31.6° and 54.3° are attributed to rhombohedral phase of MoS_2 (JCPDS #89-5112) whilst peaks at 13.4° and 35.6° are due to MoS_2 (JCPDS #37-1492) hexagonal phase. Note that, disappearance of graphitic peak (2θ = 26.9°, Curve b of Fig. 2A) indicates the change in crystallinity by formation of MoS_2 on the surface of PGE. However, Raman spectroscopy is a influential tool to inspect the structural change of graphite. In general, graphitic materials show specific D and G bands at 1330 and 1570 cm^{-1} for sp^3 and sp^2 carbon structures respectively. The intensity ratio of D and G bands, i.e., I_D/I_G is a measure for graphitic disorder (Vishnu et al., 2017, 2018). Curve a and b of Fig. 2B represents the Raman spectra of MoS_2-PGE and PGE respectively. Raman spectrum of MoS_2-PGE (Fig. 2B) shown 377 and 406 cm^{-1} peaks corresponding to typical E^1_{2g} and A_{1g} vibrational modes of MoS_2, respectively, with increase in ratio of I_D/I_G from 0.045 (PGE) to 0.092. These E^1_{2g} and A_{1g} modes are due to in-plane and out-of-plane of Mo-S vibration, respectively, (Barman et al., 2017; Jagminas et al., 2016) and the frequency difference between these two modes i.e., 29 cm^{-1} indicates the formation of > 4 layered MoS_2 on PGE surface. The broader and lower intensity of the E^1_{2g} peak denotes the presence of high number of defects in MoS_2 formed on PGE (Fan et al., 2017).

Further, XPS analysis of MoS_2-PGE (Fig. 2C) was performed to study the chemical composition and the oxidation state of the Mo. C 1s XPS spectrum exhibits three peaks around 284.5, 286.7 and 289.1 eV for sp^2 hybrid C, hydroxyl C and the carboxylic acid C of PGE respectively. Mo 3d XPS spectrum of MoS_2 displays the two peaks at 225.3 and 229.1 eV which represent the $3d_{5/2}$ and $3d_{3/2}$— electronic states of Mo and confirm + 4 oxidation state of Mo in MoS bond. Further, Mo 3d spectrum was deconvoluted into four peaks and two peaks (225.4 and 229.1 eV) reveals to the existence of metallic 1T phase of MoS_2 while other two peaks (225.4 and 231.8 eV) are ascribed to semiconducting 2H phase of MoS_2. S 2p XPS spectrum of MoS_2 displays the doublet peaks located at 161.4 and 162.7 eV are due to the $2p_{3/2}$ and $2p_{1/2}$ electronic states of the divalent sulfide ions respectively. Peaks at 161.4 and 162.7 eV are due to metallic 1T phase and peaks at 162.4 and 163.7 eV are from semiconducting 2H phase of MoS_2 (Fan et al., 2017). In addition, an extra S 2 s peak at 221.3 eV in Mo 3d XPS spectra was also witnessed the binding state of S in MoS_2. Both spectra shown lower percentage of semiconducting 2 H phase and higher percentage of the metallic 1 T phase indicating the feasibility of MoS_2-PGE towards electrochemical applications.

3.2. Electrochemical studies

Preliminary measurements were focussed to probe the electrochemical characteristics of MoS_2-PGE with respect to bare PGE. In electrochemistry, $Fe(CN)_6^{3-/4-}$ redox system is one of the standard and bench mark system to study the surface features of the modified electrode. Fig. 3A corresponds to the comparative CV responses of MoS_2-PGE (curve a) and PGE (curve b) measured at scan rate (ν) = 10 mV s^{-1} in 5 mM $Fe(CN)_6^{3-/4-}$ + 0.5 M KCl solution. A redox peak at equilibrium potential, $E_{1/2}$ ((E_{pa} + E_{pc})/2) = 0.21 V with a calculated peak-to-peak potential, $\Delta E_p = E_{pa}$-E_{pc}, where E_{pa} and E_{pc} are anodic and cathodic peak potentials, respectively, was found to be 115 mV for MoS_2-PGE; whereas, the values of PGE were 0.21 V and 139 mV. The decrement in the ΔE_p for MoS_2-PGE exhibits a facile electron-transfer behaviour of the PGE after the hydrothermal growth of MoS_2. From the obtained peak current (Fig. 3A), surface area used for electrochemical studies (A_e in cm^2) could be estimated using the standard Randle–Sevcik equation (Vishnu et al., 2017, 2018): $i_p = 2.69 \times 10^5 A_e D^{1/2} n^{3/2} \nu^{1/2} c$, where n = electron number involved during a redox reaction, D and c are the diffusion coefficient (7.6×10^{-6} cm^2 s^{-1}) and concentration of the redox species. Using the above equation, A_e of MoS_2-PGE and PGE were calculated and obtained 0.165 and 0.071 cm^2 respectively. It is obvious that the PGE contains lesser surface than the MoS_2-PGE. Similarly, electrochemical impedance spectroscopy (EIS) experiments were also done in 5 mM $Fe(CN)_6^{3-/4-}$ + 0.5 M KCl solution at an open circuit potential. Fig. 3B is comparative impedance responses (Nyquist plot, Z′ vs Z″) of MoS_2-PGE (curve a) and PGE (curve b). The impedance responses are fitted as per the Randles circuit displayed as an inset in Fig. 3B, where Z_w = Warburg impedance; C_{dl} = double layer capacitance; R_s and R_{ct} are the resistance from solution and charge transfer. The diameter of the semicircle is equal to the R_{ct} value and indicates the electron transfer kinetics of the redox probe at the interface of electrode/electrolyte (Gopalakrishnan et al., 2018). Upon hydrothermal growth of MoS_2 on PGE, R_{ct} value of PGE (957.4 Ω; Fig. 3B, curve b) is reduced to 382.7 Ω (Fig. 3B, curve a). Exchange current density (j_0) values can be calculated from the R_{ct} values obtained from Fig. 3B using $j_0 = RT/nFAR_{ct}$ (Gopalakrishnan et al., 2018; Vishnu et al., 2018). It is obvious that j_0 value of MoS_2-PGE (0.949 mA cm^{-2}) is about thrice higher than that of the PGE (0.379 mA cm^{-2}). Lower R_{ct} and higher j_0 values indicate that MoS_2-PGE acts as a good electro-catalyst for electrochemical sensing applications (Vishnu et al., 2018).

As model analytes, guanine (G) and adenine (A), two important nucleobases were chosen to explore the electrocatalytic activity of MoS_2-PGE. As seen in Fig. 4A, the bare PGE (curve b) has displayed no significant electrochemical response for the nucleobases (G and A) in pH 7.4 PBS. The observations depicts the high over potential towards the electrochemical detection of G and A on the unmodified carbon electrodes like glassy carbon electrode and PGE. On contrary, experiment with MoS_2-PGE (Curve a, Fig. 4A) showed electrochemical signals at 0.58 and 0.90 V for G and A respectively. Likewise, to confirm the analyte specific peaks, cyclic volatmmetric measurements were performed with single analyte (Figs. 4B and C). Note that, the individual analyte peak current responses (Figs. 4B and C) were exactly matching with the data obtained from simultaneous analysis (Fig. 4A). More interestingly, the MoS_2-PGE displayed 60 ± 10 and 120 ± 10 mV decrement in the over-potential for electrochemical sensing of G and A in neutral pH that the other reported electrodes (Hui et al., 2015; Thangaraj and Kumar, 2013; Wang et al., 2018; Yari and Saidikhah, 2016). This observation indicates that MoS_2-PGE is an efficient electrocatalyst for sensitive electrochemical detection of nucleobases. Meanwhile, other electrochemical methods like differential pulse voltammetry (DPV) offers separation-free and simultaneous detection of G and A by a single voltammetric run with experimental simplicity and notable sensitivity. Control DPV study with simultaneous (Fig. 4D) and discreet nucleobases (Figs. 4E and 4F) matches with the individual voltammetric peaks at 0.56 V for G and 0.85 V for A. Post analyses, MoS_2-PGE was subjected to DPV measurement in blank pH 7.4 PBS to inspect the adsorption of the analytes on MoS_2-PGE and found no strong adsorption of analyte. At optimal DPV parameters, G and A were detected in their mixture solution using the MoS_2-PGE. During the electrochemical analyses, the concentration of one analyte is changed, and other remains fixed (i.e., 25 μM). As shown in Fig. 5 MoS_2-PGE displayed systematic increments in the peak response upon increment in the concentration of analyte. DPV of the G oxidation peak current showed linearity in the range of 15–120 μM with a current sensitivity and regression coefficient values of 0.431 A M^{-1} (N = 3 devices) and 0.98 respectively (Fig. 5A) For A, the concentration linearity is

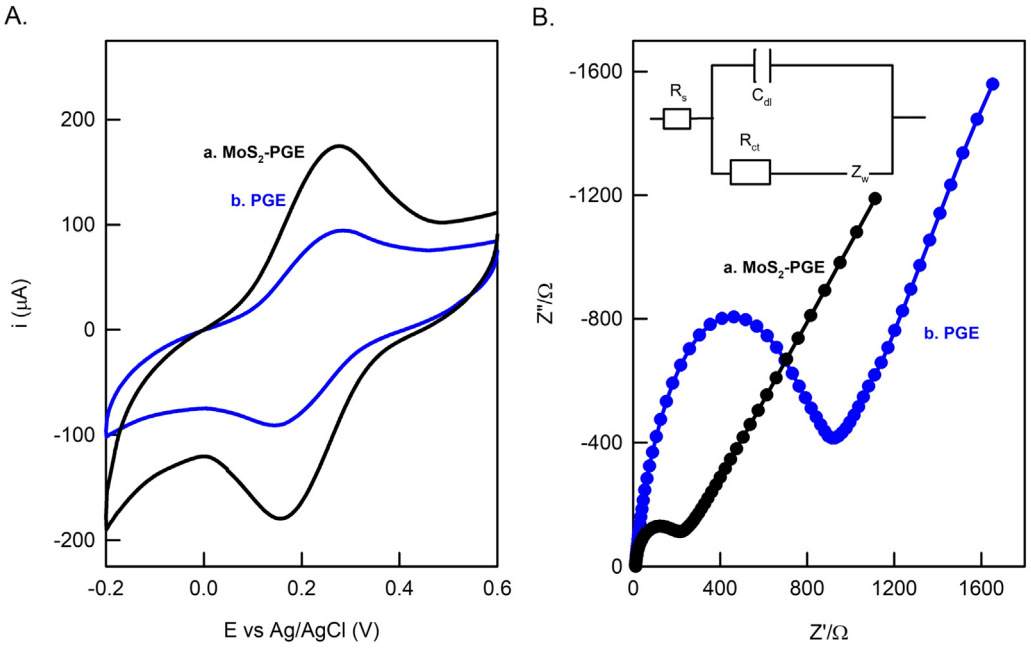

Fig. 3. (A) CV and (B) EIS responses of the MoS_2-PGE (curve a) and PGE (curve b) with 5 mM each of $Fe(CN)_6^{3-/4-}$ in 0.5 M KCl. For the CV, scan rate is 10 mV s^{-1} and for EIS, open circuit potential is 0.25 V. Inset of Fig. 3B is the Randles equivalent circuit model.

15–120 μM and sensitivity = 0.418 A M^{-1} (N = 3 devices) and regression coefficient value = 0.96 (Fig. 5B). Nine repetitive DPV measurements of 25 μM of G and A (Fig. 5) without any pretreatment and intermediate cleaning procedures were considered to examine the reproducibility of the MoS_2-PGE electrode. Interestingly the MoS_2-PGE showed low relative standard deviation (RSD) values of 3.3% and 1.1% for G and A respectively. The obtained values denote the acceptable reproducibility of MoS2-PGE towards the separation free measurmenets of G and A. Limit of detection (LOD; signal-to-noise = 3) of PGE-MoS_2 towards G and A were calculated using the obtained sensitivity and standard deviation values as 0.76 and 2.38 μM respectively. Displayed analytical performance is comparable and even superior to some of the

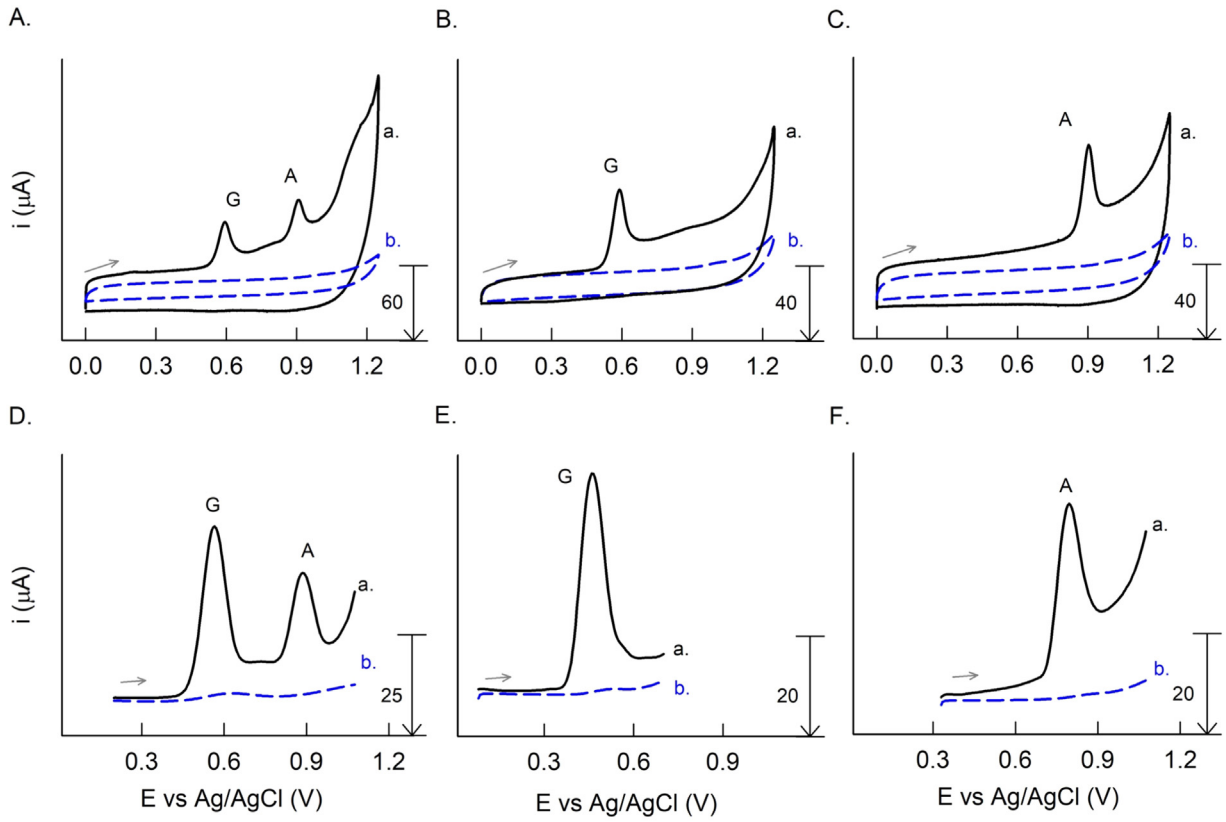

Fig. 4. Simultaneous and discrete CV (A) and DPV (B) responses of a mixture containing G (100 μM) and A (75 μM) at MoS_2-PGE (curve a) and PGE (curve b) in pH 7.4 PBS. CV scan rate is 50 mV s^{-1}. DPV parameters: increment potential = 0.004 V; amplitude = 0.05 V; pulse width = 0.2 s; pulse period = 0.5 s.

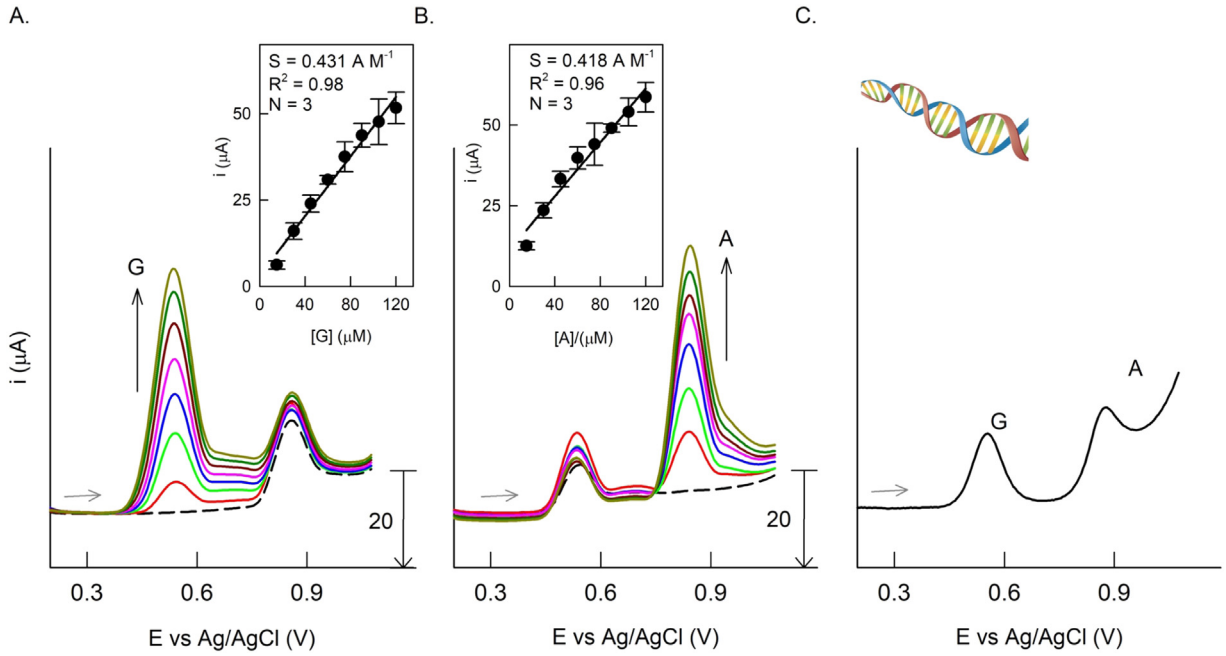

Fig. 5. Typical DPV responses for the simultaneous detection of G and A with respect to one fixed analyte on MoS_2-PGE in pH 7.4 PBS (A and B). Plots of i vs analyte concentration were given as respective inset figures. DPV response of MoS_2-PGE for the detection of G and A in Calf-Thymus DNA sample in pH 7.4 PBS (C). DPV parameters: Initial potential = 0.2 V; final potential = 1.1 V; increment potential = 0.004 V; amplitude = 0.05 V; pulse width = 0.2 s; pulse period = 0.5 s.

Table 1
Comparison of the analytical performance shown by different electrochemical sensors used for G and A analyses.

Electrochemical sensors	Tech.	pH	Guanine (G)			Adenine (A)			Ref.
			Linear range (μM)	Sens. (A M^{-1})	LOD (μM)	Linear range (μM)	Sens. (A M^{-1})	LOD (μM)	
Au-rGO/MWCNT/graphite	SWV	7.0	13–165	0.026	3.30	15–185	0.012	3.70	Ng and Khor (2017)
Cu@Ni-MWCNT/GCE	DPV	3.0	1–180	0.410	0.17	2–150	0.438	0.33	Wang et al. (2018)
TAN-AgNP-PANI/CPE	DPV	6.0	0.9–140	0.021	3.00	1.0–200	0.044	2.80	Yari and Saidikhah (2016)
GMC/GCE	DPV	7.0	15–200	0.289	0.76	25–150	0.262	0.63	Thangaraj and Kumar (2013)
AgNPs-β-CD-Gr/GCE	DPV	3.7	0.3–200	0.084	0.09	0.5–250	0.071	0.15	Hui et al. (2015)
MWCNT-Fe_3O_4 @PDA-Ag/CPE	DPV	4.0	8–130	0.300	4.80	10–120	0.438	2.90	Yari and Derki (2016)
Activated GCE	DPV	4.5	5–230	0.014	0.50	20–230	0.017	0.50	Li et al. (2016)
MoS_2-PGE	DPV	7.4	15–120	0.431	0.76	15–120	0.418	2.38	**This work**

MWCNT = multiwalled carbon nanotube; Fe_3O_4 = iron oxide; PDA = polydopamine; Ag = silver; CPE = carbon paste electrode; Au = gold; rGO = reduced graphene oxide; TAN = trithiane; NP = nanoparticle; PANI = polyaniline; GMC = graphitized mesoporous carbon; CD = cyclodextrin;Gr = graphene; GCE = glassy carbon electrode; Cu = copper; Ni = nickel; SWV = square wave voltammetry.

existing literature reports (Table 1) (Hui et al., 2015; Li et al., 2016; Ng and Khor, 2017; Thangaraj and Kumar, 2013; Yari and Saidikhah, 2016; Yari and Derki, 2016; Wang et al., 2018). Thus, the fabricated electrode is suitable for separation free and sensitive detection of G and A. Simplicity in fabrication and easy regeneration of electrode surface are added advantages to our novel and low cost electrode. In order to validate the practical data given by the proposed electrode, the G and A contents of a commercially available Calf Thymus DNA sample was determined by standard addition approach. Fig. 5C is the DPV response of DNA sample using MoS_2-PGE electrochemical sensor. As noticed, well-defined peaks were because of G and A oxidation. Table S1 comprises the analytical information obtained from the Fig. 5C. Measured concentrations of G and A are 25. 05 and 21.51 μM and their ratio is 0.85 and this value is parallel with the recent reported literature (Table S2; Hui et al., 2015; Thangaraj and Kumar, 2013; Yari and Saidikhah, 2016; Wang et al., 2018). Finally, calculated recovery values were ~100%. Although very few reports are available on MoS_2 composite synthesised by multiple steps for detection of G and A (Yang et al., 2015a, 2015b). Interestingly, MoS_2 was hydrothermally grown on pencil electrode in a single step here which promotes development of a clean room and lithography-free fabrication approach for an ultra-low-cost electrode (~$ 0.04; Table S3). Moreover, the low-cost sensor offers several advantages in terms of LOD and sensitivity. Overall, the developed sensor will be an enticing material in the future electrochemical analysis on gene diagnostics.

4. Conclusions

MoS_2-PGE was prepared by simple hydrothermal growth of MoS_2 on PGE. Physicochemical characterization of MoS_2-PGE revealed the formation of MoS_2 on PGE with high metallic phase and electrochemical analyses also suggested MoS_2-PGE is useful in electroanalytical applications. In physiological pH, the MoS_2-PGE displayed a sharp, well-defined and well-separated oxidation peaks corresponding to the simultaneous detection of G and A. Under optimal differential pulse voltammetric (DPV) conditions, analyses of two analytes (G and A) simultaneously exhibited linear calibration plots in the range of 15–120 μM. More interestingly, the MoS_2-PGE can be subjected to repetitive DPV measurements of G and A without any pretreatment and intermediate cleaning procedures. The sensitivity and LOD are better than the previous reports and it can be extended for real time diagnostics. Thus, practicability of such MoS_2-PGE was examined by

measurement of G and A in commercially available Calf-Thymus DNA. The obtained G and A concentration ratio ([G]/[A] = 0.85) which is parallel to the standard value. Obtained recovery values from the DNA sample analyses were near to 100% indicating the accessibility and efficiency of the presented electrode for other biological samples. Though the current approach is a proof-of-concept, the developed sensor will fetch new frontiers in development of affordable devices for broad range of bio-applications in the near future.

Acknowledgements

NV thanks Department of Science and Technology-Science and Engineering Research Board, India sponsored National Post-Doctoral Fellowship (PDF/2017/001447) for the financial support.

Conflicts of interest

There are no conflicts of interest.

Appendix A. Supporting information

Supplementary data associated with this article can be found in the online version at doi:10.1016/j.bios.2018.08.055.

References

Arvand, M., Khoshkholgh, Z., Hemmati, S., 2018. J. Electroanal. Chem. 817, 149–159.
Barman, B.K., Das, D., Nanda, K.K., 2017. J. Mater. Chem. A 5 (34), 18081–18087.
Barua, S., Dutta, H.S., Gogoi, S., Devi, R., Khan, R., 2018. ACS Appl. Nano Mater. 1 (1), 2–25.
Chu, Y., Cai, B., Ma, Y., Zhao, M., Ye, Z., Huang, J., 2016. RSC Adv. 6 (27), 22673–22678.
Fan, D.H., Niu, D.J., Huang, K.J., 2010. Sens. Actuator B-Chem. https://doi.org/10.1016/j.snb.2010.03.023.
Fan, X., Gaddam, R.R., Kumar, N.A., Zhao, X.S., 2017. Adv. Energy Mater. 7 (19).
Gopalakrishnan, A., Sha, R., Vishnu, N., Kumar, R., Badhulika, S., 2018. Nano-Struct. Nano-Obj. 16, 96–103.
Hirao, I., Kimoto, M., Yamashige, R., 2012. Acc. Chem. Res. 45 (12), 2055–2065.
Huang, Y., Guo, J., Kang, Y., Ai, Y., Li, C.M., 2015. Nanoscale 7 (46), 19358–19376.
Hui, Y., Ma, X., Hou, X., Chen, F., Yu, J., 2015. Ionics 21 (6), 1751–1759.
Jagminas, A., Niaura, G., Žalnėravičius, R., Trusovas, R., Račiukaitis, G., Jasulaitiene, V., 2016. Sci. Rep. 6, 37514.
Li, H., Wang, X., Wang, Z., Zhao, W., 2016. J. Solid State Chem. 20 (8), 2223–2230.
Li, X., Li, W., Li, M., Cui, P., Chen, D., Gengenbach, T., Chu, L., Liu, H., Song, G., 2015. J. Mater. Chem. A 3 (6), 2762–2769.
Nandi, D.K., Sahoo, S., Sinha, S., Yeo, S., Kim, H., Bulakhe, R.N., Heo, J., Shim, J.J., Kim, S.H., 2017. ACS Appl. Mater. Interfaces 9 (46), 40252–40264.
Ng, K.L., Khor, S.M., 2017. Anal. Chem. 89 (18), 10004–10012.
Pradhan, S., Biswas, S., Das, D.K., Bhar, R., Bandyopadhyay, R., Pramanik, P., 2018. New J. Chem. 42 (1), 564–573.
Randviir, E.P., Banks, C.E., 2012. RSC Adv. 2 (13), 5800–5805.
Sahatiya, P., Jones, S.S., Badhulika, S., 2018. Flex. Print. Electron. 3, 015002.
Sun, T., Li, Z., Liu, X., Ma, L., Wang, J., Yang, S., 2016. J. Power Sources 331, 180–188.
Thangaraj, R., Kumar, A.S., 2013. J. Solid State Chem. 17 (3), 583–590.
Thangaraj, R., Nellaiappan, S., Sudhakaran, R., Kumar, A.S., 2014. Electrochim. Acta 123, 485–493.
Vishnu, N., Gandhi, M., Rajagopal, D., Kumar, A.S., 2017. Anal. Methods 9 (15), 2265–2274.
Vishnu, N., Gopalakrishnan, A., Badhulika, S., 2018. Electrochim. Acta 269, 274–281.
Wang, D., Huang, B., Liu, J., Guo, X., Abudukeyoumu, G., Zhang, Y., Ye, B., Li, Y., 2018. Biosens. Bioelectron. 102, 389–395.
Wetmur, J.G., 1991. Crit. Rev. Biochem. Mol. Biol. 26 (3–4), 227–259.
Yang, T., Chen, M., Nan, F., Chen, L., Luo, X., Jiao, K., 2015a. J. Mater. Chem. B 3 (24), 4884–4891.
Yang, T., Yang, R., Chen, H., Nan, F., Ge, T., Jiao, K., 2015b. ACS Appl. Mater. Interfaces 7 (4), 2867–2872.
Yari, A., Derki, S., 2016. Sens. Actuator B-Chem. 227, 456–466.
Yari, A., Saidikhah, M., 2016. J. Electroanal. Chem. 783, 288–294.
Yin, H., Zhou, Y., Ma, Q., Ai, S., Ju, P., Zhu, L., Lu, L., 2010. Process Biochem. 45 (10), 1707–1712.
Zhang, J., Liu, S., Liang, H., Dong, R., Feng, X., 2015. Adv. Mater. 27 (45), 7426–7431.